Journal of Materials Chemistry B

ROYAL SOCIETY OF CHEMISTRY

PAPER

View Article Online
View Journal | View Issue

Cite this: J. Mater. Chem. B, 2024, 12, 1624

β-Glycosidase sensitive oral nanoparticles for combined photothermal and chemo treatment of colorectal cancer†

Jingning Zhou,‡[a] Zequn Zhuang,‡[a] Rui Gao,[b] Ran Li[c] and Yigang Chen*[a]

Colorectal cancer is one of the most common malignant tumors in the world, and its treatment strategies mainly include surgical resection, chemotherapy, adjuvant radiotherapy, and immunotherapy. Among them, chemotherapy inevitably produces systemic toxicity due to the lack of tumor targeting properties and drug resistance caused by long-term medication frequently occurs, immensely constraining the efficacy of chemotherapy alone. To solve the above-mentioned problems, rhamnolipid was used to encapsulate the chemotherapeutic drug 5-FU and photothermal agent bismuthene nanosheets (BiNS), chitosan was applied as the shell of the nanoparticle, and BiNS@RHL-CS/5-FU NPs for oral administration was successfully prepared. When transported in the stomach and small intestine, the double protection of rhamnolipid and chitosan shell prevented the early release of BiNS and 5-FU. When transported to the colon, β-glycosidase existing in the microenvironment along with elevated pH degraded the chitosan shell, and the reduction in particle size was beneficial for tumor tissue to uptake nanoparticles, thus greatly improving the tumor targeting ability of 5-FU and reducing the systemic toxicity. Due to the presence of BiNS, 1.0 W cm^{-2} 808 nm laser irradiation significantly increased the temperature of the tumor site, not only killing tumor cells directly but also promoting cell uptake and penetration of nanoparticles in the tumor tissue, accelerating the release of 5-FU and improving the sensitivity of tumor cells to chemotherapy, eventually solving the shortcomings of traditional chemotherapy alone. Excellent anti-tumor efficacy has been achieved in both *in vitro* and *in vivo* experiments.

Received 13th October 2023,
Accepted 19th December 2023

DOI: 10.1039/d3tb02393a

rsc.li/materials-b

Introduction

Colorectal cancer is one of the most common malignant tumors in the world. With the improvement of people's living standards and the acceleration of industrialization, the incidence and mortality of colorectal cancer are rising rapidly.[1,2] The main treatment methods for colorectal cancer currently include surgical resection, chemotherapy, adjuvant radiotherapy, and immunotherapy, among which chemotherapy is still the main strategy to inhibit tumor growth or metastasis.[3] However, single chemotherapy usually results in drug resistance and systemic side effects.[4] In recent years, photothermal therapy (PTT) have shown great potential in cancer treatment owing to its advantages of strong specificity and few side effects.[5] PTT generated by photothermal nanomaterials can convert light energy into heat energy under external near-infrared light irradiation, which can raise the temperature to damage the tumor cells. However, due to the limited transmission, single PTT cannot penetrate deep into organisms and kill tumor cells completely.[6,7] Therefore, the strategy of combining two or more treatment methods has been widely used. Among them, combined chemotherapy and photothermal therapy for colon cancer can not only kill tumor cells through different mechanisms but also reduce side effects.[8]

Two-dimensional nanosheets have attracted widespread attention in the field of biomedicine, especially in the treatment of cancer.[9] Bismuth is a metal material with low toxicity and relatively low price, which has advantages of safety and economy in *in vivo* application.[10,11] Bismuthene nanosheets with high specific surface area can efficiently load small molecule chemotherapeutic agents and possess excellent photothermal conversion efficiency for photothermal therapy.[12] At

[a] Department of General Surgery, The Affiliated Wuxi No. 2 People's Hospital of Nanjing Medical University, 68 Zhongshan Road, Wuxi, 214002, Jiangsu, China. E-mail: 9862023226@jiangnan.edu.cn
[b] School of Pharmacy, China Pharmaceutical University, Nanjing, 211100, Jiangsu, China
[c] School of Pharmacy, Jiangsu University, Zhenjiang, 212013, Jiangsu, China

† Electronic supplementary information (ESI) available. See DOI: https://doi.org/10.1039/d3tb02393a

‡ These authors contributed equally to this work and should be considered co-first authors.

present, the drug delivery systems of photothermal therapy combined with chemotherapy are mostly administrated by intravenous injection. While oral colon drug delivery systems can not only improve patient compliance but also increase drug concentrations in the colon and reduce the dosage of drug administration.[13] Studies found that colon tissue can absorb beneficial nutrients through microbiota. Besides, the extremely long retention time in the colon also provides good conditions for the absorption of drugs.[14] Many polymeric materials, such as chitosan, inulin, guar gum, and pectin,[15,16] can be degraded by the enzymes produced by these beneficial microbes. Due to the lack of corresponding enzymes in the upper digestive tract, these materials can hardly be degraded to avoid chemotherapeutics release before reaching the colon site and allow more drugs to be released at the tumor site.[17,18] Chitosan is a kind of long chain polysaccharide extracted from the deacetylation process of chitin, and the amino group in its molecule would become positively charged under acidic conditions.[19] In addition, it can also be modified onto various nanocarrier surfaces by its strong adhesion, enhancing the penetration and adhesion to tissues, regulating cell interactions, and improving the oral bioavailability of drugs.[20,21] However, it is difficult for chitosan to completely wrap two-dimensional nanosheets without chemical crosslinking agents so that rhamnolipid nanoparticles were used in this study to encapsulate two-dimensional nanosheets and drugs. Rhamnolipid (RHL) is a non-toxic anionic biosurfactant that can be used under extreme conditions such as abnormal pH and salinity.[22,23] Its amphiphilic molecular structure can self-assemble in water to form hydrophobic core vesicles,[24] which have been used to encapsulate a variety of insoluble drugs, such as tacrolimus, dexamethasone, and curcumin.[25] Huang *et al.*[26] used RHL to encapsulate black phosphorus nanosheets (BP) and isolinderalactone (ISL) for drug-resistant *H. pylori* (*H. pylori*-R) treatment

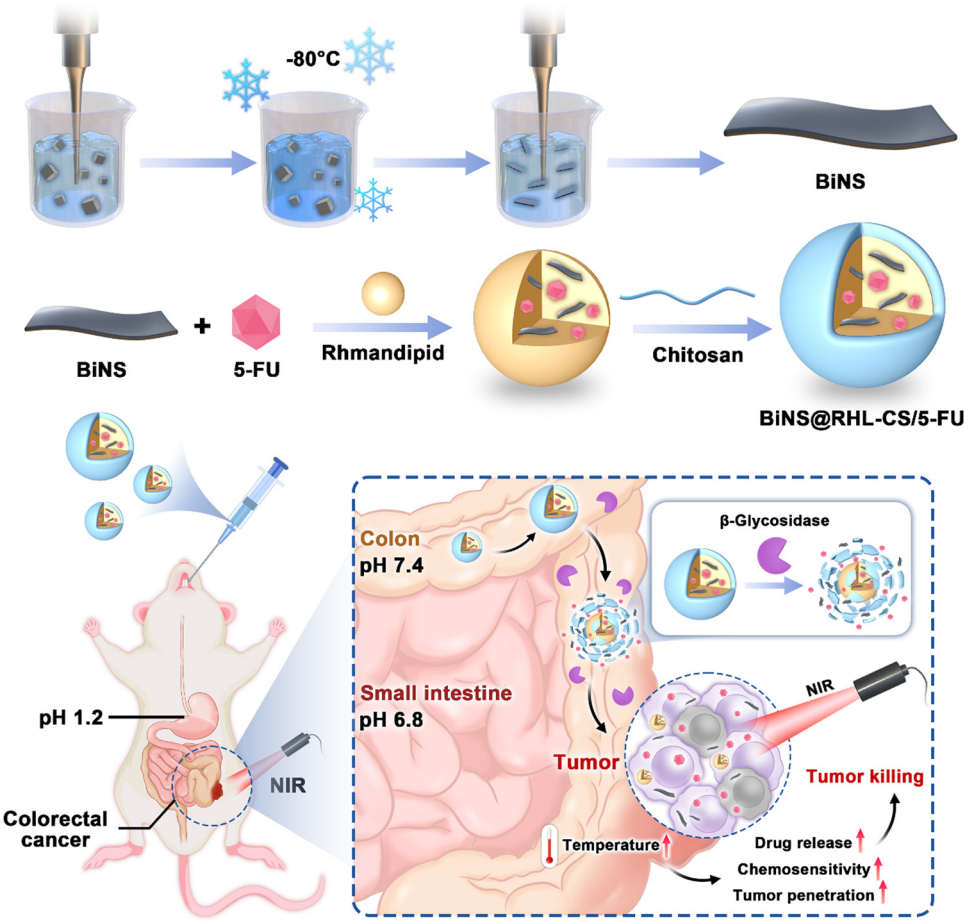

Scheme 1 In this work, we developed an oral drug delivery system BiNS@RHL-CS/5-FU NPs to combine chemotherapy and photothermal therapy together for the treatment of colorectal cancer. 5-Fluorouracil was utilized as the chemotherapeutic drug and bismuthene nanosheets (BiNS) as the photothermal agent. In order to protect the stability of BiNS and 5-FU in the gastrointestinal tract, BiNS and 5-FU were firstly wrapped in rhamnolipid nanoparticles through self-assembly. Inspired by specific enzymes secreted by colonic microbiota, chitosan (CS) was modified on the surface of nanoparticles by charge interaction. The double protection of rhamnolipid nanoparticle and the outer layer of chitosan prevented BiNS and 5-FU from being degraded in the gastrointestinal tract. β-Glycosidase existing in the colonal microenvironment can degrade the chitosan shell, and the reduction in particle size was beneficial for the tumor tissue to uptake nanoparticles, thus greatly improving the tumor targeting ability of 5-FU and reducing systemic toxicity. Photothermal therapy not only killed the tumor cells directly but also promoted the penetration of nanoparticles in the tumor tissue, accelerated the release of 5-FU, and improved the sensitivity of tumor cells to chemotherapy, eventually solving the shortcomings of traditional single chemotherapy.

by oral administration combined with chemotherapy and photothermal therapy. The RHL@BP/ISL effectively prevented the rapid degradation of black phosphorus nanosheets and drugs in the acidic stomach environment, and the photothermal instability of RHL could achieve the controlled release of drugs.

In this work, we developed an oral drug delivery system BiNS@RHL-CS/5-FU NPs to combine chemotherapy and photothermal together for the treatment of colorectal cancer. 5-Fluorouracil was utilized as the chemotherapeutic drug and BiNS as the photothermal agent. To protect the stability of BiNS and 5-FU in the gastrointestinal tract, BiNS and 5-FU were firstly wrapped in rhamnolipid nanoparticles through self-assembly. Inspired by specific enzymes secreted by colonic microbiota, chitosan (CS) was modified on the surface of nanoparticles by charge interaction. The double protection of rhamnolipid nanoparticle and the outer layer of chitosan prevented BiNS and 5-FU from being degraded in the gastrointestinal tract. β-Glycosidase existing in the colonal microenvironment degraded the chitosan shell, and the reduction in particle size was beneficial for tumor tissue to uptake nanoparticles, thus greatly improving the tumor targeting ability of 5-FU and reducing the systemic toxicity. Photothermal therapy not only killed tumor cells directly but also promoted the penetration of nanoparticles in the tumor tissue, accelerated the release of 5-FU, and improved the sensitivity of tumor cells to chemotherapy, eventually solving the shortcomings of traditional single chemotherapy. The antitumor activity studies *in vitro* and *in vivo* demonstrated that BiNS@RHL-CS/5-FU NPs had good photothermal conversion efficiency and synergistically had good antitumor efficacy. This study provided a new approach for the oral application of bismuth-based two-dimensional materials in the field of cancer treatment (Scheme 1).

Methods and materials

HPLC analysis of 5-FU

5.0 mg 5-fluorouracil was added in a 50 mL volumetric bottle and dissolved by 50 mL mobile phase (water–methanol, 95 : 5). The concentration of 5-FU in the reserve solution was 100 μg mL^{-1}. Then, the 5-FU solution was accurately prepared with concentrations of 0.2, 0.5, 1, 5, 10, 15, and 20 μg mL^{-1}. The concentration of 5-FU was detected according to the following chromatographic conditions. Standard curve was drawn with the concentration of 5-fluorouracil as the horizontal coordinate and the corresponding peak area as the vertical coordinate (Fig. S1, ESI†).

Chromatographic column: Shim-pack GIS C18 (4.6 × 250 mm, 5 μm)

Mobile phase: water (pH adjusted to 3.5 with 0.05 mol L^{-1} phosphoric acid solution) – methanol (95 : 5, v/v)

Column temperature: 40 °C

Flow rate: 1.0 mL min^{-1}

Sample size: 10 μL

Detection wavelength: 266 nm

Preparation of BiNS

300 mg bismuth powder was added to 60 mL ethanol and ultrasonicated with a power of 500 W in an ice bath for 8 h. After ultrasonication, the suspension was centrifuged for 30 min at 12 000 rpm. The collected precipitate was suspended with 40 mL deionized water and frozen overnight at −80 °C. After natural thawing, the water was removed by centrifugation, and 60 mL ethanol was added for a second probe ultrasonication for 8 h. After ultrasonication, the suspension was centrifuged at 3000 rpm for 10 min to remove the bulk bismuth powder. The supernatant was centrifuged at 12 000 rpm for 30 min. The obtained bismuthene nanosheets were suspended with 5 mL deionized water and placed in the freeze-drying machine to obtain the bismuthene nanosheets (BiNS).

Preparation of BiNS@RHL-CS/5-FU NPs

15 mg rhamnolipids and 1.5 mg 5-FU were added to 0.75 mL (0.75 g) BiNS ethanol suspension. Ultrasonication was carried out for 30 min, and 2 mL PBS solution (10 mM, pH 7.4) was slowly added under ultrasonic conditions. After that, the suspension was shaken at 37 °C with a rotating speed of 120 rpm for 1 h. The above suspension was slowly added to the chitosan solution with a concentration of 2 mg mL^{-1} (10 mL in total) and stirred for another 2 h. The suspension was transferred to a dialysis bag (WMCO = 3500) for 24 h at room temperature to remove organic solvents and free drugs. After dialysis, the suspension was centrifuged at 3500 rpm for 5 min to remove the unwrapped BiNS. BiNS@RHL-CS/5-FU NPs, which was obtained after freeze drying.

TEM

The suspension of BiNS and BiNS@RHL-CS/5-FU NPs with the concentration of 1 mg mL^{-1} was prepared for TEM. After ultrasonication, 2 μL suspension was added to the surface of the carbon-coated copper mesh after 10-fold dilution with deionized water. After standing for 2 min, the excess liquid was removed by a filter paper. Phosphotungstic acid solution was added to the surface of the copper mesh and stained for 2 min. The sample was transferred to the infrared lamp for drying, and then the microstructure was observed by TEM.

Encapsulation rate and drug loading capacity of 5-FU

BiNS@RHL-CS/5-FU NPs suspension was added in chromatographic methanol to destroy the nanostructure by ultrasonication. For detecting the drug loading capacity and encapsulation rate of 5-FU, the suspension was transferred to the inner tube of 3 kD ultrafiltration centrifuge tube. After centrifugation at 7000 rpm for 30 min, the outer tube solution was diluted with the mobile phase and then filtered by a 0.22 μm filter membrane. The content of 5-FU in the nanoparticles was determined by high performance liquid chromatography (HPLC). The content of 5-FU in the nanoparticles was determined by high performance liquid chromatography (HPLC). The mobile phases of 5-FU were composed of methanol (0.05 mol L^{-1} trifluoroacetic acid):water (95 : 5, v/v) at a flow

rate of 1.0 mL min^{-1}, and the detection wavelengths were set at 266 nm. The 5-FU content in nanoparticles was calculated according to the standard HLPC curve of 5-FU in Fig. S1 (ESI†), and the input amount of 5-FU was 1.5 mg. The encapsulation ratio of 5-FU was calculated as followed.

$$\text{Encapsulation rate (\%)} = \text{drug content in nanoparticles/drug input} \times 100\%$$

$$\text{Drug loading capacity (\%)} = \text{drug content in nanoparticles/weight of BiNS@RHL-CS/5-FU NPs} \times 100\%.$$

Photothermal performance of BiNS@RHL-CS NPs

The photothermal performance of BiNS, BiNS@RHL NPs, and BiNS@RHL-CS NPs suspension containing the same concentration of BiNS (100 μg mL^{-1}) were investigated to examine whether the modification of BiNS affected the photothermal conversion performance while the PBS solution served as the blank control. An 808 nm (1.0 W cm^{-2}) laser was used to irradiate the center of the suspension for 10 min. An infrared thermal imager was used to detect the temperature every 30 s. The photothermal performance of BiNS@RHL-CS NPs containing different concentrations of BiNS (0, 25, 50, 100 μg mL^{-1}) irradiated with 1.0 W cm^{-2} 808 nm lasers or the BiNS@RHL-CS NPs containing fixed concentration of BiNS (100 μg mL^{-1}) irradiated with 0.5 W cm^{-2}, 1.0 W cm^{-2}, and 1.5 W cm^{-2} 808 nm lasers were determined by the same method mentioned above.

The stability of the photothermal effect of BiNS@RHL-CS NPs was investigated by the on/off cycle experiment. 1 mL BiNS@RHL-CS NPs suspension containing 100 μg mL^{-1} BiNS was transferred in a 1.5 mL EP tube. 1.0 W cm^{-2} 808 nm laser was utilized to irradiate the center of the suspension for 5 min. An infrared thermal imager was used to detect the maximum temperature in the irradiated area every 30 s. After the end of irradiation, the suspension cooled naturally for 5 min. Four cyclic experiments were carried out, and the photothermal change curve was drawn.

In vitro release study mimicking gastrointestinal conditions

4 mL BiNS@RHL-CS/5-FU NPs suspension was transferred to a dialysis bag (MWCO = 3500) and then the bag was placed into beakers containing 36 mL simulated gastric fluid (SGF) with pH 1.2, simulated intestinal fluid (SIF) with pH 6.8, and simulated colon fluid (SCF) with pH 7.4, respectively (two portions of SCF did not contain β-glycosidase and another two portions contained β-glycosidase, 5 U mL^{-1}), and the dialysis bag was allowed to be completely immersed in the release medium. The beaker was put at a constant temperature shaker with a temperature of 37 °C with a rotating speed of 120 rpm. 2 mL release medium was quantitatively removed at different time points (0.5, 1, 2, 3, 4, 6, 8, 10, 12, 24, 36, 48 h) and the corresponding release medium with the same volume and temperature was immediately added. In addition, two samples immersed in SCF with (Blue line in Fig. 3A) or without β-glycosidase (green line in Fig. 3A) were irradiated with 1.0 W cm^{-2} 808 nm laser for 5 min at specified time points. Samples collected at each time point were filtered by a filter membrane, and the drug concentrations in the release medium were determined by HPLC. The release curves of BiNS@RHL-CS/5-FU NPs under different media were plotted according to the statistics.

To further investigate the effects of near-infrared irradiation and β-glucosidase on drug release, 4 mL BiNS@RHL-CS/5-FU NPs suspension was transferred in a dialysis bag (MWCO = 3500). The dialysis bags were placed in beakers containing 36 mL simulated gastric fluid with pH 1.2, immersed in the release medium, and placed in a constant temperature shaker with a temperature of 37 °C with a rotating speed of 120 rpm. After the period, all SGF was removed and replaced by 36 mL simulated intestinal fluid (pH 6.8). Two hours later, all SIF was removed and replaced by 36 mL simulated colonic fluid. The period lasted for 24 h. The 4#SCF did not contain β-glycosidase; the 3#SCF contained β-glycosidase; the 2#SCF did not contain β-glycosidase but was irradiated with 1.0 W cm^{-2} 808 nm laser for 5 min; the 1#SCF contained β-glycosidase (5 U mL^{-1}) and was irradiated with 1.0 W cm^{-2} 808 nm laser for 5 min. 2 mL release medium was removed at different time points (0.5, 1, 2, 2.5, 3, 3.5, 4, 6, 8, 10, 12, 24 h) and fresh release medium was immediately added with the same volume and temperature. The irradiation started at the time point of 4 h.

Biocompatibility of BiNS@RHL-CS NPs

BiNS@RHL-CS NPs was diluted to 5 μg mL^{-1}, 10 μg mL^{-1}, 25 μg mL^{-1}, 50 μg mL^{-1}, and 100 μg mL^{-1} by DMEM medium. HT29 cells were seeded in a 96-well plate with a concentration of 5.0×10^4 cells mL^{-1} (100 μL per well). 100 μL diluted BiNS@RHL-CS NPs was added to each well to replace the former medium and cultured for 24 h. 10 μL CCK-8 solution was added to each well and incubated for 2 h. The OD value was measured at 450 nm wavelength. The cell survival rate was calculated as follows.

$$\text{Relative cell viability (\%)} = (OD_{target} - OD_{blank})/(OD_{Control} - OD_{blank}) \times 100\%$$

Cell uptake

In this experiment, BiNS@RHL-CS/C6 NPs were prepared with a fluorescent probe C6 instead of 5-FU. HT29 cells were seeded in a 24-well plate and incubated for 24 h. Five sample groups were set up: (1) control group; (2) BiNS@RHL-CS/C6 NPs group; (3) BiNS@RHL-CS/C6 NPs + NIR irradiation group; (4) BiNS@RHL-CS/C6 NPs (β-glycosidase, 5 U mL^{-1}) group; (5) BiNS@RHL-CS/C6 NPs (β-glycosidase, 5 U mL^{-1}) + NIR irradiation group. In groups 4 and 5, BiNS@RHL-CS/C6 NPs were pre-incubated with β-glycosidase for 1 h before administration to simulate the degradation of outer chitosan *in vivo*. Groups 3 and 5 were irradiated with 808 nm (1.0 W cm^{-2}) laser for 5 min. After incubation for 4 h, the cells were washed with PBS solution 3 times and fixed with 4% paraformaldehyde for 30 min. The

nucleus was stained with 5 μg mL^{-1} DAPI for 5 min. The cell uptake of HT29 was observed by a fluorescence microscope.

In vitro antitumor efficacy

The experiment was divided into: (1) control group; (2) NIR group; (3) BiNS@RHL-CS NPs group; (4) free 5-FU group; (5) BiNS@RHL-CS/5-FU NPs group; (6) BiNS@RHL-CS NPs + NIR irradiation group; (7) BiNS@RHL-CS/5-FU NPs + NIR irradiation group; (8) BiNS@RHL-CS/5-FU NPs (β-glycosidase, 5 U mL^{-1}) group; (9) BiNS@RHL-CS/5-FU NPs (β-glycosidase, 5 U mL^{-1}) + NIR irradiation group. Cells in groups 2, 6, 7, and 9 were irradiated with 808 nm (1.0 W cm^{-2}) laser for 5 min. Groups 8 and 9 were incubated with β-glycosidase for 1 h before administration. The dose of BiNS in BiNS@RHL-CS/5-FU NPs was approximately 100 μg mL^{-1}, and the dose of 5-FU was approximately 190 μg mL^{-1}. The relative cell viabilities were calculated according to the above method.

In vivo antitumor efficacy

All animal experiments were performed in compliance with the relevant laws and guided by Animal Ethics Review Committee of The Affiliated Wuxi No. 2 People's Hospital of Nanjing Medical University.

Healthy female NOD/SCID mice (6–8 weeks of age, 18–20 g) were selected, and 100 μL cell suspension was inoculated on the right axillary of the mice. Follow-up experiments were performed when the tumor volume was about 150–200 mm^3. The animals were managed according to procedures approved by Jiangsu University.

The suspension of BiNS@RHL-CS/DiR NPs was firstly prepared. Three tumor-bearing mice were randomly selected and given intragastric administration at a dose of 200 μL per mouse (the dose of DiR was 1 mg kg^{-1}). Biodistribution analysis was performed at 1, 8, 18, and 24 h after administration with a small animal live imager (λ_{ex} = 748 nm, λ_{em} = 780 nm). After 24 h, tumor and major organs (heart, liver, spleen, lung, and kidney) were harvested, and the distribution of DiR in tumor and organ tissues was observed.

To study the photothermal properties of BiNS@RHL-CS/5-FU NPs *in vivo*, tumor-bearing mice were randomly divided into two groups with 3 mice in each group, such as group 1: PBS group and group 2: BiNS@RHL-CS/5-FU NPs (dose of BiNS was approximately 8 mg kg^{-1} and dose of 5-FU was approximately 15 mg kg^{-1}). The mice were anesthetized with 4% chloral hydrate 24 h after intragastric administration. 1.0 W cm^{-2} 808 nm laser was used to irradiate the tumor site for 5 min. Thermal images of the tumor site were taken by an infrared thermal imager every one minute. Finally, line charts of the photothermal performance of BiNS@RHL-CS/5-FU NPs *in vivo* were drawn with time as the horizontal coordinate and the temperature at the tumor site as the vertical coordinate.

The administration strategy was as follows: (1) PBS group, the dose was 200 μL/20 g; (2) 5-FU group, the volume of administration was 200 μL/20 g and the dose of 5-FU was 15 mg kg^{-1}; (3) BiNS@RHL-CS/5-FU NPs group, the administration volume was 200 μL/20 g; (4) BiNS@RHL-CS/5-FU NPs + NIR group, 1.0 W cm^{-2} 808 nm laser irradiated the tumor site for 5 min. The dose of BiNS in groups 3 and 4 was approximately 8 mg kg^{-1}, and the dose of 5-FU was 15 mg kg^{-1}. All drugs were administered by gavage every two days. The total treatment period was 14 days. Mice were killed on the next day after the last administration. Tumor tissues and major organs (heart, liver, spleen, lung, and kidney) were collected and fixed in 4% paraformaldehyde tissue solution. H&E staining, TUNEL analysis, and Ki67 assay were performed.

Results and discussion

Characterization of BiNS@RHL-CS NPs

The micro-morphologies of BiNS and BiNS@RHL-CS/5-FU NPs were observed by transmission electron microscopy. As shown in Fig. 1A, it was observed that after the shattering process combined with ultrasonic liquid phase stripping and freezing, the two-dimensional nanosheets with a transverse diameter in the range of 100–200 nm were obtained. The more transparent the layers, the smaller the thickness of the nanosheets, indicating that bismuth powder had been successfully stripped into ultra-thin two-dimensional nanosheets. BiNS were coated with a film structure after modification, and the edges became smooth and round. The average particle size of BiNS was 132.62 nm. The size of BiNS@RHL NPs increased to 194.50 nm, and the value of BiNS@RHL-CS NPs increased from 194.50 nm to 264.08 nm after CS modification (Fig. 1B). The increase in the particle size was due to the modifications of rhamnolipids and CS. The average particle size of BiNS@RHL-CS/5-FU NPs increased from 264.08 nm to 270.45 nm after 5-FU loading. The particle size and PDI remained stable for 72 h (Fig. S2, ESI†), demonstrating the excellent long-term stability of BiNS@RHL-CS/5-FU NPs. The zeta potential of the BiNS of BiNS@RHL-CS NPs was −6.22 mV, and the value for BiNS@RHL NPs coated with rhamnolipids further decreased to −12.93 mV. With the further modification of chitosan, the zeta potential of BiNS@RHL-CS NPS changed from −12.93 mV to +15.93 mV. The zeta potential of BiNS@RHL-CS/5-FU NPs slightly decreased from +15.93 mV before drug loading to +15.11 mV (Fig. 1C), which provided an important basis for the successful construction of BiNS@RHL-CS/5-FU NPs. The encapsulation rate and drug loading capacity of 5-FU were 84.99% and 3.45%, respectively. FTIR was used to further verify the structure of the prepared BiNS@RHL-CS/5-FU NPs. As shown in Fig. 1D and E, BiNS@RHL NPs, BiNS@RHL-CS NPs, and BiNS@RHL-CS/5-FU NPs all showed a wide absorption peak at 3600–3100 cm^{-1}, which was caused by the stretching vibration of O–H and N–H bonds in rhamnolipids. There are two characteristic absorption peaks at 2930 cm^{-1} and 2851 cm^{-1} caused by the C-H stretching vibration of CH_2 in RHL. The absorption spectrum of BiNS@RHL NPs shows that the infrared characteristic peak of BiNS is partly covered by RHL. BiNS@RHL NPs exhibited both the characteristic peak of RHL in general and the characteristic peak of BiNS in some regions, indicating the successful synthesis of BiNS@RHL NPs.

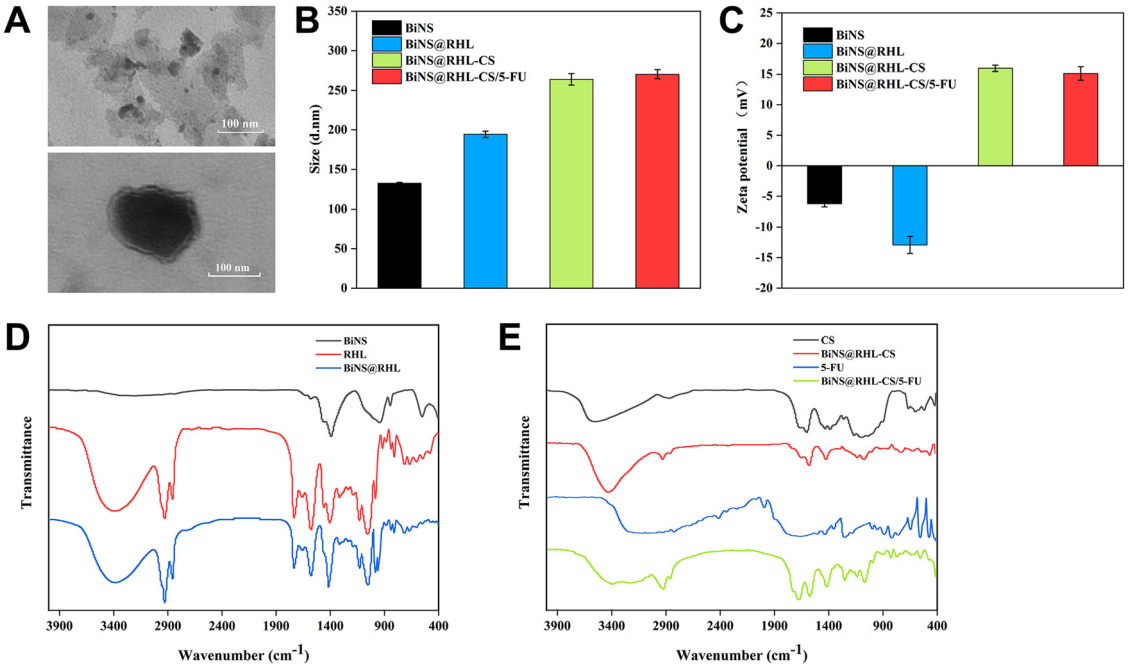

Fig. 1 Characterization of BiNS@RHL-CS NPs. (A) TEM image of BiNS (up) and BiNS@RHL-CS/5-FU NPs (down). Scale bar is 100 nm. Particle size (B) and zeta potential (C) of BiNS, BiNS@RHL NPs, BiNS@RHL-CS NPs, and BiNS@RHL-CS/5-FU NPs. FT-IR spectra of BiNS, RHL, BiNS@RHL NPs (D), CS, BiNS@RHL-CS NPs, 5-FU, and BiNS@RHL-CS/5-FU NPs (E).

The infrared absorption spectra of BiNS@RHL-CS NPs after chitosan modification showed that two characteristic absorption peaks appeared at 1655 cm^{-1} and 1569 cm^{-1}, which belonged to the amide I and amide II bands in chitosan, respectively. The characteristic bands at 1253–992 cm^{-1} including the stretching vibration of C–O–H, symmetric stretching vibration of C–O–C, and asymmetric stretching vibration of C–O–C belonged to the rhamnose ring in the RHL structure. Several absorption characteristic peaks of 5-FU could be observed in the infrared spectrum of BiNS@RHL-CS/5-FU NPs. The characteristic peaks at 1426 cm^{-1}, 884 cm^{-1}, 815 cm^{-1}, and 759 cm^{-1} were caused by the vibration of the carbon-fluorine bond (–CF═CH–) in 5-FU so that the existence of 5-FU in the nanoparticles was proved. The FT-IR experiment results further verify the successful construction of BiNS@RHL-CS/5-FU NPs.

In vitro photothermal performance of BiNS@RHL-CS NPs

The photothermal conversion performance of BiNS, BiNS@RHL NPs, and BiNS@RHL-CS NPs suspensions containing bismuthene nanosheets with the same concentration were investigated. Under the irradiation of 1.0 W cm^{-2} 808 nm near-infrared laser, the temperature of 100 μg mL^{-1} BiNS suspension increased from 23.2 °C to 47 °C and 51.7 °C within 5 min and 10 min, respectively. Compared with 100 μg mL^{-1} BiNS suspension, the photothermal conversion efficiency of BiNS@RHL NPs and BiNS@RHL-CS NPs decreased slightly, but the temperature variation was still much greater than that for 50 μg mL^{-1} BiNS suspension (Fig. 2A). However, the temperature of the PBS solution in the control group hardly changed under the same condition. To conclude, BiNS@RHL NPs and BiNS@RHL-CS NPs still had excellent photothermal performance after modification.

Subsequently, we investigated whether the photothermal performance of BiNS@RHL-CS NPs was dependent on the concentration of the BiNS contained or the power of the 808 nm laser. As shown in Fig. 2B, with the increase in the concentration of BiNS contained in BiNS@RHL-CS NPs, the temperature increased significantly under 1.0 W cm^{-2} irradiation. Likewise, the change in temperature was tightly correlated with the power of the 808 nm laser under a fixed concentration of BiNS (Fig. 2C). This article was based on the treatment temperature required for photothermal agents to induce cancer cell death. Considering that excessive temperature would cause thermal damage to normal tissues, we chose BiNS@RHL-CS NPs containing 100 μg mL^{-1} BiNS; the power of the laser was 1.0 W cm^{-2}, and the irradiation time was 5 min for subsequent *in vitro* and *in vivo* experiments.

Finally, the photothermal stability curve of BiNS@RHL-CS NPs containing 100 μg mL^{-1} BiNS were investigated under 1.0 W cm^{-2} 808 nm laser irradiation. During the four "on/off" cycles, BiNS@RHL-CS NPs reached the highest temperatures of 48.4 °C, 49.3 °C, 48.5 °C, and 49.1 °C within 5 min (Fig. 2D), revealing that BiNS@RHL-CS NPs had excellent photothermal stability.

In vitro drug release study of BiNS@RHL-CS NPs

β-Glycosidase was introduced to simulate the colonic microenvironment so that it was urgent to determine its concentration used in following experiments. We incubated different

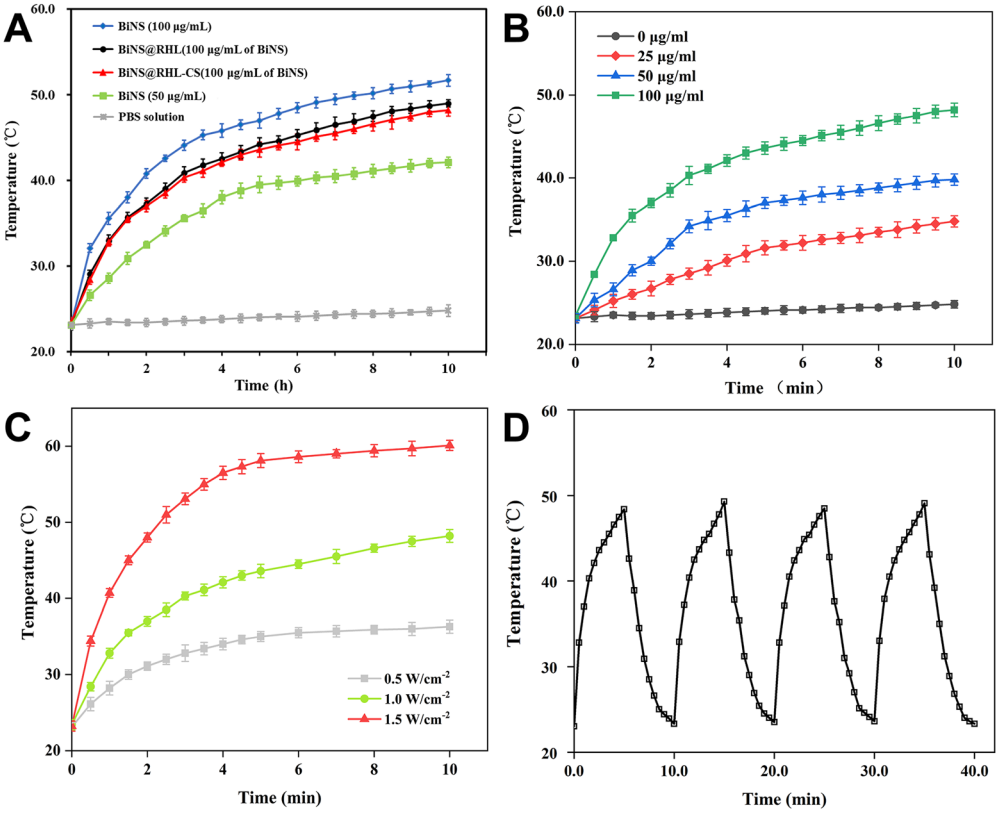

Fig. 2 *In vitro* photothermal performance of BiNS@RHL-CS NPs. (A) Temperature-changing curves of PBS solution, BiNS (50 μg mL^{-1}), BiNS@RHL NPs (100 μg mL^{-1} of BiNS), BiNS@RHL-CS NPs (100 μg mL^{-1} of BiNS), and BiNS (100 μg mL^{-1}) suspensions under 1.0 W cm^{-2} 808 nm laser irradiation. Concentration (B) and irradiation power (C)-dependent temperature-changing curves. (D) Temperature circulation curves of BiNS@RHL-CS NPs suspension under 808 nm laser irradiation.

concentrations of β-glycosidase with BiNS@RHL-CS/5-FU NPs at 37 °C and determined the particle sizes to explore the optimal enzyme concentration of β-glycosidase. As shown in Fig. S3 (ESI†), the particle size of the nanoparticles decreased significantly after co-incubation with enzymes for 1 h, which was related to the degradation of the outermost chitosan. According to the results, β-glycosidase with a concentration of 5 U mL^{-1} was selected as the enzyme concentration.

To explore the release characteristics of BiNS@RHL-CS/5-FU NPs, this study simulated different pH and conditions along the gastrointestinal tract, whether β-glycosidase existed, and whether 808 nm laser irradiation was performed. As shown in Fig. 3A, the cumulative drug release percentage of BiNS@RHL-CS/5-FU NPs in simulated gastric fluid (SGF) at pH 1.2 (black line) within 48 h was 21.6%. The value in simulated intestine fluid (SIF, pH 6.8) (orange line) and simulated colonic fluid (SCF, pH 7.4) (grey line) reached 31.9% and 38.5%, respectively, which was possibly due to the reduced protonation degree of surface modified chitosan in slightly acidic or neutral medium, thus weakening the charge interaction between the chitosan and the nanoparticles, leading to the more release of 5-FU. The cumulative release percentage of 5-FU significantly increased in the SCF containing β-glycosidase (yellow line), suggesting that the presence of β-glycosidase in the colon destroyed the chitosan shell and promoted drug release. It was worth noting that SCF with NIR irradiation (green line) showed more drug release rate than SCF with β-glycosidase (yellow line) and SCF without β-glycosidase (grey line), illustrating that the increase in temperature directly led to enhanced drug release. The cumulative 5-FU release rate at 48 h of SCF with β-glycosidase increased to 78.1% after NIR laser irradiation (blue line), indicating that combining the existence of β-glycosidase and raise in temperature together significantly promoted drug release.

For better simulating the release behavior of 5-FU in the stomach, small intestine, and colon, different release times in different release medium were set according to the transport time of food in different segments of the gastrointestinal tract. As shown in Fig. 3B, the cumulative release percentage in SGF and SIF ranged from 30–40%. After 24 h release in SCF without β-glycosidase, the cumulative release percentage was only 46.1%; Under the condition of SCF containing β-glucosidase, the value increased to 57.4% as the chitosan shell of BiNS@RHL-CS/5-FU NPs was degraded by β-glucosidase. However, under near-infrared irradiation, the cumulative release percentage of the drug increased to 61.7% (without β-glucosidase, green line) and 79.8% (with β-glucosidase, blue line) due to the photothermal effect generated by bismuthene nanosheets under 808 nm irradiation.

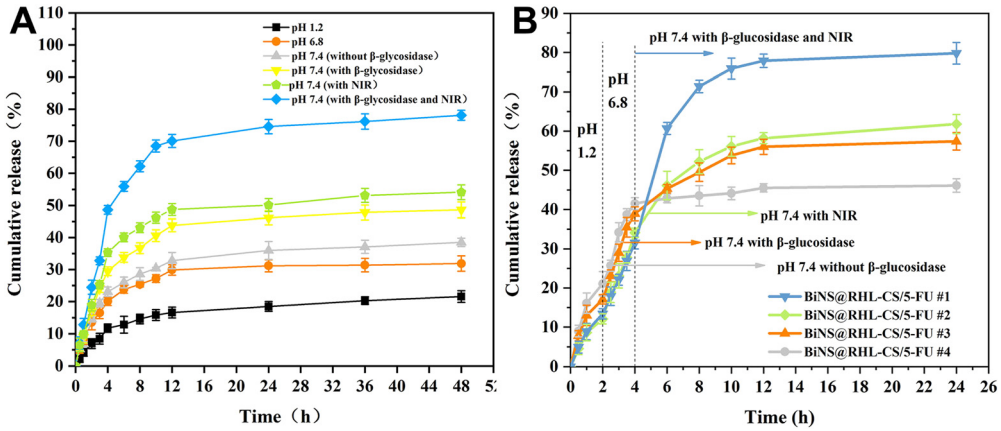

Fig. 3 Release behavior of BiNS@RHL-CS/5-FU NPs. (A) Cumulative release of 5-FU treated with different pH, with or without β-glycosidase and NIR, n = 3. (B) Cumulative release of 5-FU by simulating the processes in the gastrointestinal tract under different treatments.

In vitro antitumor efficacy

Before studying the cytotoxicity of BiNS@RHL-CS NPs, it is necessary to confirm its biocompatibility. As shown in Fig. 4A, HT29 cells were incubated with different concentrations of BiNS@RHL-CS NPs for 24 h, and when the concentration reached 100 μg mL^{-1}, the survival rate of HT29 cells was still higher than 94%, indicating that the blank nanoparticles prepared in this study have no cytotoxicity in the concentration range of 0–100 μg mL^{-1}, thus showing superb biocompatibility.

To further investigate the antitumor activity of BiNS@RHL-CS/5-FU NPs *in vitro*, we used the hydrophobic fluorescent dye coumarin 6 instead of 5-FU to observe HT29 uptake under different conditions. As shown in Fig. 4B, the fluorescence intensity of the BiNS@RHL-CS/C6 NPs group with β-glycosidase incubation was higher than that of the bare BiNS@RHL-CS/C6 NPs group, indicating that the degradation of the chitosan shell led to more cell uptake due to the smaller particle size and C6 release. In addition, after laser irradiation, the fluorescence intensity of both the groups was significantly higher than that of the correlated groups without irradiation. The explanation for this phenomenon might because the increase in temperature promoted C6 release and enhanced

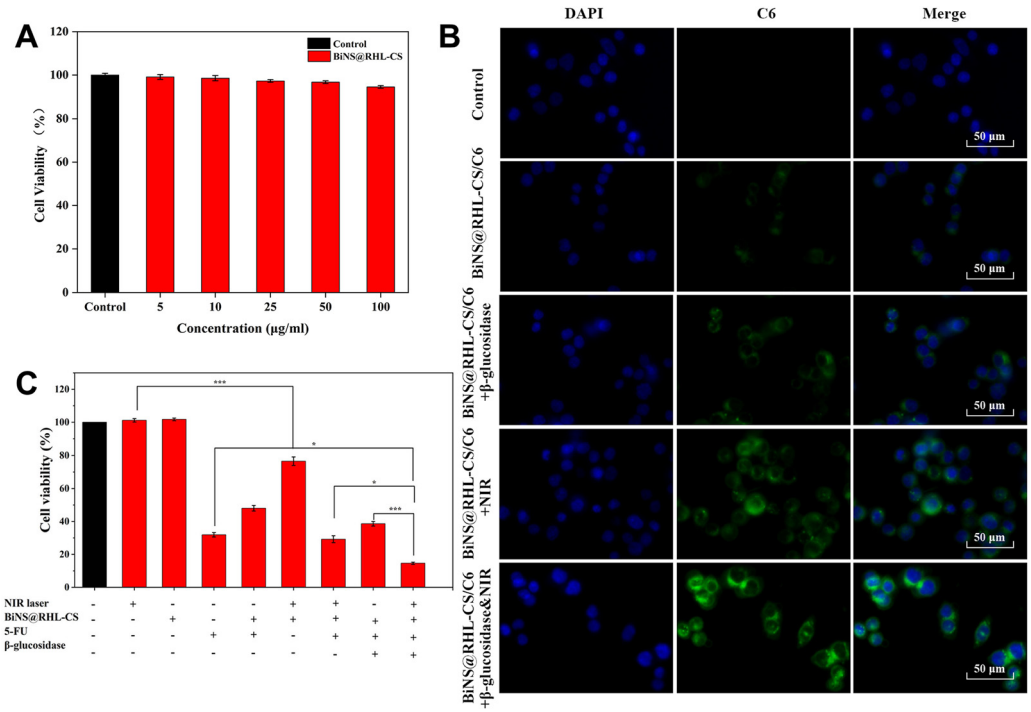

Fig. 4 *In vitro* anti-tumor efficacy. (A) Relative cell viability of HT29 cells after co-incubating with BiNS@RHL-CS NPs for 24 h, n = 4. (B) Cell uptake of BiNS@RHL-CS/C6 NPs with different treatments. Scale bar is 50 μm. Images were taken by inverted fluorescence microscope. (C) Relative cell viability of HT29 cells with different treatments, n = 4. Significant differences were analyzed by One-way Anova, *, $0.01 < p < 0.05$, *** $p < 0.001$.

the permeability of the cell membrane, thus promoting cell uptake.

The antitumor activities of 5-FU, BiNS@RHL-CS NPs, and BiNS@RHL-CS/5-FU NPs under different treatments were investigated by the CCK-8 assay. As shown in Fig. 4C, laser irradiation or blank BiNS@RHL-CS NPs alone had little effect on cell survival. However, after laser irradiation on BiNS@RHL-CS NPs, the cell survival rate decreased to 77.56%, indicating that the photothermal effect exhibited a certain antitumor effect. The survival rate of HT29 treated with the combination of BiNS@RHL-CS/5-FU NPs, laser irradiation, and β-glycosidase decreased to 14.63%. The antitumor efficacy was significantly better than that of free 5-FU, BiNS@RHL-CS/5-FU NPs without laser irradiation and β-glycosidase incubation, BiNS@RHL-CS/5-FU NPs without laser irradiation or β-glycosidase incubation, demonstrating that chemotherapy combined with photothermal therapy had a stronger killing effect on tumor cells.

Biodistribution of BiNS@RHL-CS/5-FU *in vivo*

We investigated the targeting ability of BiNS@RHL-CS/5-FU for tumor tissues, and the cell membrane dye DiR was used as a fluorescent marker instead of 5-FU to obtain BiNS@RHL-CS/DiR. As shown in Fig. 5A, the fluorescence signals in mice is mainly distributed in the gastrointestinal tract, and with the extension of the oral administration time, the fluorescence signals in the gastrointestinal tract of mice gradually decreased, while the fluorescence intensity in the tumor site gradually increased. After 24 h, more fluorescence signals are still accumulated in the tumor site due to the EPR effect. 24 h after administration, the fluorescence images of the tumor tissues and major organs (heart, liver, spleen, lung, and kidney) were collected. As shown in Fig. 5B, fluorescence signals were observed for the tumor, liver, and kidney tissues, further demonstrating that BiNS@RHL-CS/DiR NPs can precisely target the tumor tissue after oral administration.

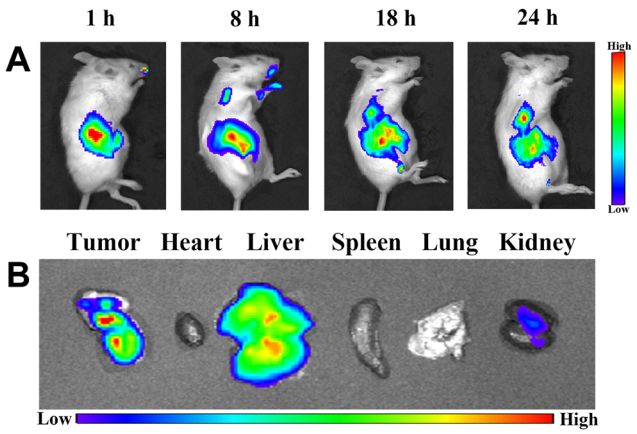

Fig. 5 Biodistribution of BiNS@RHL-CS/5-FU *in vivo*. (A) *In vivo* fluorescence distribution after oral administration of BiNS@RHL-CS/DiR NPs at different time points. (B) *Ex vivo* fluorescence distribution images of tumor, heart, liver, spleen, lung, and kidney dissected from tumor-bearing mice sacrificed 24 h after drug administration.

In vivo antitumor efficacy

The photothermal effect of BiNS@RHL-CS/5-FU NPs accumulated in the tumor tissues after systemic circulation was investigated. As shown in Fig. 6A, the temperature of the PBS group only increased by 2.1 °C within 5 min, indicating that NIR laser irradiation alone could not effectively improve the temperature of the tumor site. However, the temperature of BiNS@RHL-CS/5-FU NPs increased from 32.4 °C to 44.6 °C with the extension of irradiation time (Fig. 6B), indicating that BiNS@RHL-CS/5-FU NPs had good photothermal conversion performance *in vivo*.

The changes in the tumor volume with different administrations are shown in Fig. 6C. The tumors in the PBS group had the fastest growth rate, reaching 1160.2 mm^3 in 14 days. However, free 5-FU group, BiNS@RHL-CS/5-FU NPs group, and BiNS@RHL-CS/5-FU NPs+NIR irradiation group can effectively inhibit the growth of tumor volume. At the initial stage of treatment, there was no significant difference in the tumor growth inhibition rate among the three groups. The tumor growth rate in the free 5-FU group significantly increased 4 days after administration while the growth rate in the BiNS@RHL-CS/5-FU NPs group and the BiNS@RHL-CS/5-FU NPs+NIR group was relatively slow as the double-layer protection of rhamnose-lipid nanoparticles and chitosan layer reduced the early degradation of the drug in the stomach. After 8 days of administration, the tumor inhibition efficacy of the BiNS@RHL-CS/5-FU+NIR group was significantly better than that of the BiNS@RHL-CS/5-FU group. Under near-infrared laser irradiation, the photothermal effect produced by BiNS not only inhibited the growth of tumor cells but also enhanced drug penetration at the tumor site. The changes in the tumor size in mice were consistent with the results of the *in vitro* tumor diagram of mice 14 days after administration (Fig. 6D), indicating that the antitumor effect of the BiNS@RHL-CS/5-FU NPs drug delivery system combined with chemotherapy and photothermal therapy was superior to that of chemotherapy alone.

H&E, TUNEL, and Ki67 staining of tumor tissues are shown in Fig. 6E. H&E staining results showed that almost no significant tumor cell necrosis areas were observed in the PBS group while necrosis areas were observed in other groups to some degree. The necrosis area in the BiNS@RHL-CS/5-FU+NIR group was significantly greater than that in the BiNS@RHL-CS/5-FU group. Similarly, TUNEL results showed that the cell apoptosis rate was the highest in the BiNS@RHL-CS/5-FU+NIR group. Ki67 results showed that the proliferation activity of tumor cells in the BiNS@RHL-CS/5-FU+NIR group was significantly lower than that in other groups. The results of the three tests were consistent with the changes in the tumor volume in mice, jointly proving that the BiNS@RHL-CS/5-FU NPs drug delivery system combined with photothermal therapy and chemotherapy can improve the antitumor efficacy.

Finally, we investigated the *in vivo* biocompatibility of BiNS@RHL-CS/5-FU. The average body weight of mice in the PBS group increased from 19.0 g before administration to 21.4 g (Fig. S4, ESI†). The average body weight of mice in the

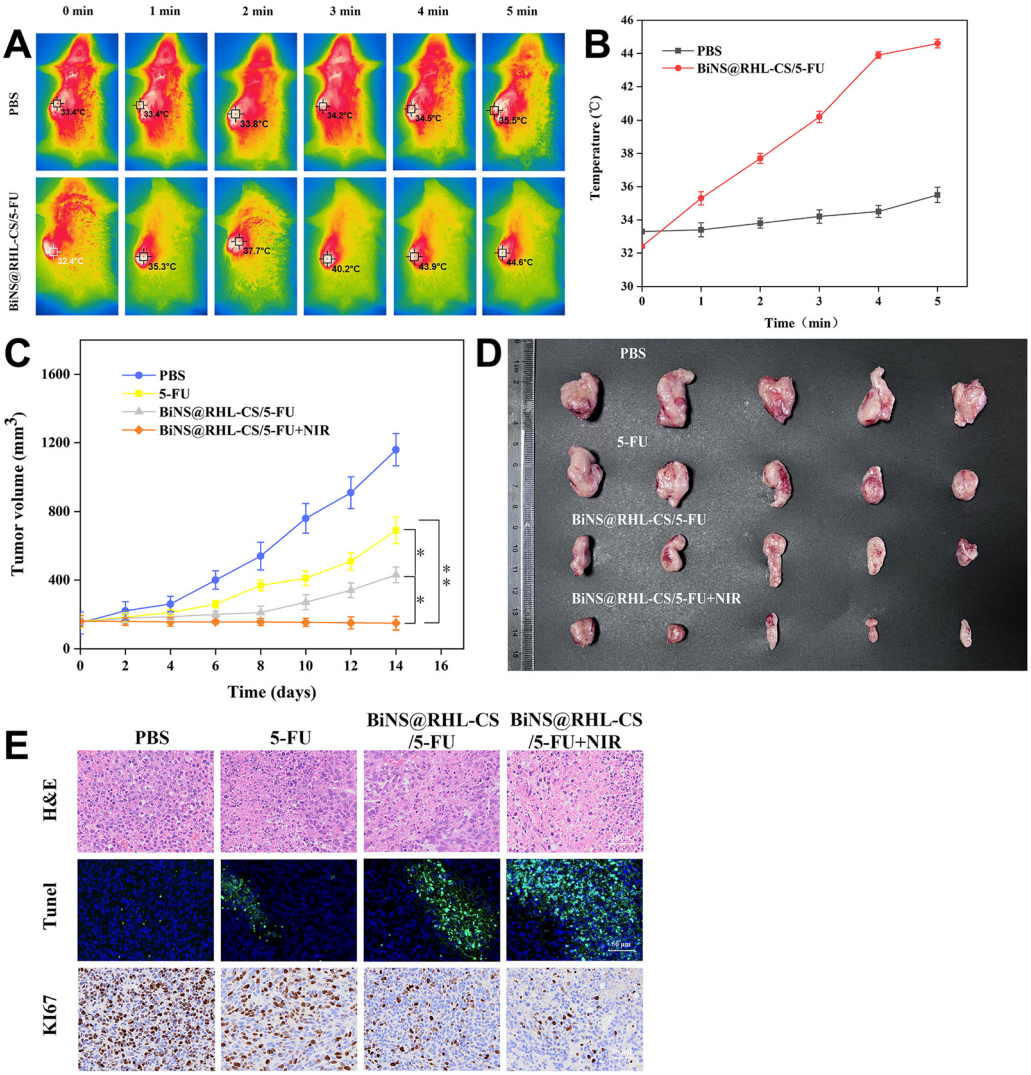

Fig. 6 *In vivo* anti-tumor efficacy. (A) *In vivo* infrared thermal images under 808 nm laser irradiation (1.0 W cm^{-2}). (B) Temperature change curves obtained from (A). (C) The curves of tumor volumes after various treatments within 14 days, $n = 5$. Significant differences were analyzed by One-way Anova, *, $0.01 < p < 0.05$, **, $p < 0.01$. (D) Images of tumor tissues sacrificed at the end of the treatment. (E) H&E, TUNEL, and Ki67 analysis of tumor tissues.

free drug 5-FU group increased slightly during the first two doses and decreased after the third dose, which may be related to the toxic side effects of 5-FU on the gastrointestinal tract. The average body weight of mice increased slightly after 10 days of administration, which may be due to the weight gain caused by the growth of tumors in mice. The mean body weight of tumor-bearing mice in the BiNS@RHL-CS/5-FU NPs group and the BiNS@RHL-CS/5-FU NPs+NIR group increased slightly from the initial body weight after 14 days of administration, indicating that the toxic side effects of free drugs encapsulated in the nanoparticles can be reduced *in vivo*. Major organs of mice in each group were collected for H&E staining, and the results showed that there were no significant lesions in the heart, liver, spleen, lung, and kidney of mice in each group under the treatment regimen (Fig. S5, ESI†), thus demonstrating the safety of BiNS@RHL-CS NPs as a drug carrier *in vivo*.

Conclusions

In this research, we successfully developed BiNS@RHL-CS/5-FU NPs for the oral treatment of colon cancer in combination with chemotherapy and photothermal therapy. A novel two-dimensional bismuthene nanoparticle was used as the photothermic agent, and 5-fluorouracil, a commonly used chemotherapy drug, was encapsulated in rhamnose-lipid nanoparticles through self-assembly to enhance the stability of 5-FU and BiNS. Moreover, to prevent the early release of 5-FU and BiNS in the gastrointestinal tract, we were inspired by the specific enzymes secreted by the colon flora, and the BiNS@RHL-CS/5-FU NPs oral drug delivery system was successfully constructed by modifying chitosan on the surface of nanoparticles through charge interaction. The chitosan shell protected the inner BiNS@RHL/5-FU in the stomach and small intestine with low pH value through electrostatic adsorption. When it transferred to the colon with

pH 7.4, the protonation degree of chitosan decreased, and together in the presence of β-glucosidase, the particle size significantly reduced, which was beneficial for cell uptake and tumor tissue penetration. The following PTT not only killed the tumor cells directly but also further promoted cell uptake, tissue penetration, and 5-FU release. So far, we have developed a nano drug delivery system with synergistic treatment effects for the enhanced treatment of colorectal cancer. Excellent antitumor efficacy has been achieved both in *in vitro* and *in vivo* experiments. More importantly, the orally administrated dosage was convenient for medication, reducing the pain caused by intravenous injection and greatly enhancing the compliance of medication. We believe that BiNS@RHL-CS/5-FU NPs is an ideal oral antitumor drug delivery system.

Ethical statement

All animal experiments were performed in compliance with the relevant laws and guided by Animal Ethics Review Committee of The Affiliated Wuxi No. 2 People's Hospital of Nanjing Medical University.

.

Conflicts of interest

There are no conflicts to declare.

Acknowledgements

This study was funded by the Project of Wuxi Science and Technology Development Fund (Y20212004) and the Wuxi Taihu Lake Talent Plan, Team in Medical and Health Profession, 2021.

References

1 H. G. Welch and D. J. Robertson, Colorectal Cancer on the Decline–Why Screening Can't Explain It All, *N. Engl. J. Med.*, 2016, **374**(17), 1605–1607.
2 M. Riihimäki, A. Hemminki and J. Sundquist, *et al.*, Patterns of metastasis in colon and rectal cancer, *Sci. Rep.*, 2016, **6**, 29765.
3 Nanodiamond based multifunctional platform for oral chemo-photothermal combinational therapy of orthotopic colon cancer.
4 L. B. Vong, T. Yoshitomi and H. Matsui, *et al.*, Development of an oral nanotherapeutics using redox nanoparticles for treatment of colitis-associated colon cancer, *Biomaterials*, 2015, **55**, 54–63.
5 D. Jaque, L. Martinez Maestro and B. Del Rosal, *et al.*, Nanoparticles for photothermal therapies, *Nanoscale*, 2014, **6**(16), 9494–9530.
6 Z. Zha, S. Zhang, Z. Deng, Y. Li, C. Li and Z. Dai, Enzyme-responsive copper sulphide nanoparticles for combined photoacoustic imaging, tumor-selective chemotherapy and photothermal therapy, *Chem. Commun.*, 2013, **49**(33), 3455–3457, DOI: 10.1039/c3cc40608c.
7 Y. Xing, T. Ding and Z. Wang, *et al.*, Temporally Controlled Photothermal/Photodynamic and Combined Therapy for Overcoming Multidrug Resistance of Cancer by Polydopamine Nanoclustered Micelles, *ACS Appl. Mater. Interfaces*, 2019, **11**(15), 13945–13953.
8 Z. Li, Y. Chen and Y. Yang, *et al.*, Recent Advances in Nanomaterials-Based Chemo-Photothermal Combination Therapy for Improving Cancer Treatment, *Front. Bioeng. Biotechnol.*, 2019, **7**, 293.
9 H. Lin, S. Gao and C. Dai, *et al.*, A Two-Dimensional Biodegradable Niobium Carbide (MXene) for Photothermal Tumor Eradication in NIR-I and NIR-II Biowindows, *J. Am. Chem. Soc.*, 2017, **139**(45), 16235–16247.
10 X. Ma, Y. Zhao and X. J. Liang, Theranostic nanoparticles engineered for clinic and pharmaceutics, *Acc. Chem. Res.*, 2011, **44**(10), 1114–1122.
11 S. L. Gorbach, Bismuth therapy in gastrointestinal diseases, *Gastroenterology*, 1990, **99**(3), 863–875.
12 Y. Zhu, Y. Q. Wu and S. S. Li, *et al.*, Photocatalytic and photothermal bismuthene nanosheets as drug carrier capable of generating CO to improve drug sensitivity and reduce inflammation for enhanced cancer therapy, *Chem. Eng. J.*, 2022, 446.
13 T. Plyduang, L. Lomlim and S. Yuenyongsawad, *et al.*, Carboxymethylcellulose-tetrahydrocurcumin conjugates for colon-specific delivery of a novel anti-cancer agent, 4-amino tetrahydrocurcumin, *Eur. J. Pharm. Biopharm.*, 2014, **88**(2), 351–360.
14 M. Naeem, U. A. Awan and F. Subhan, *et al.*, Advances in colon-targeted nano-drug delivery systems: challenges and solutions, *Arch. Pharmacal Res.*, 2020, **43**(1), 153–169.
15 S. Amidon, J. E. Brown and V. S. Dave, Colon-targeted oral drug delivery systems: design trends and approaches, *AAPS PharmSciTech*, 2015, **16**(4), 731–741.
16 V. R. Sinha and R. Kumria, Polysaccharides in colon-specific drug delivery, *Int. J. Pharm.*, 2001, **224**(1–2), 19–38.
17 L. Mei, Z. Zhang and L. Zhao, *et al.*, Pharmaceutical nanotechnology for oral delivery of anticancer drugs, *Adv. Drug Delivery Rev.*, 2013, **65**(6), 880–890.
18 E. Moroz, S. Matoori and J. C. Leroux, Oral delivery of macromolecular drugs: Where we are after almost 100years of attempts, *Adv. Drug Delivery Rev.*, 2016, **101**, 108–121.
19 I. A. Lima, N. M. Khalil and T. T. Tominaga, *et al.*, Mucoadhesive chitosan-coated PLGA nanoparticles for oral delivery of ferulic acid, *Artif. Cells Nanomed. Biotechnol.*, 2018, **46**(sup2), 993–1002.
20 M. S. Alai, W. J. Lin and S. S. Pingale, Application of polymeric nanoparticles and micelles in insulin oral delivery, *J. Food Drug Anal.*, 2015, **23**(3), 351–358.
21 L. A. Frank, G. R. Onzi and A. S. Morawski, *et al.*, Chitosan as a coating material for nanoparticles intended for biomedical applications, *Reactive Funct. Polym.*, 2020, **147**, 104459.
22 C. A. Marangon, V. C. A. Martins and M. H. Ling, *et al.*, Combination of Rhamnolipid and Chitosan in Nanoparticles

Boosts Their Antimicrobial Efficacy, *ACS Appl. Mater. Interfaces*, 2020, **12**(5), 5488–5499.

23 G. Yi, J. Son and J. Yoo, *et al.*, Rhamnolipid nanoparticles for in vivo drug delivery and photodynamic therapy, *Nanomedicine*, 2019, **19**, 12–21.

24 O. Pornsunthorntawee, S. Chavadej and R. Rujiravanit, Characterization and encapsulation efficiency of rhamnolipid vesicles with cholesterol addition, *J. Biosci. Bioeng.*, 2011, **112**(1), 102–106.

25 Y. Ma, S. Chen and W. Liao, *et al.*, Formation, Physicochemical Stability, and Redispersibility of Curcumin-Loaded Rhamnolipid Nanoparticles Using the pH-Driven Method, *J. Agric. Food Chem.*, 2020, **68**(27), 7103–7111.

26 Y. Q. Huang, R. J. Li and Y. Y. Dai, *et al.*, Rhamnolipid-assisted black phosphorus nanosheets with efficient isolinderalactone loading against drug resistant Helicobacter pylori, *Mater. Des.*, 2022, **216**, 110536.